Polyaniline-Multiwalled Carbon Nanotube Composites: Characterization by WAXS and TGA

T. Jeevananda,[1] Siddaramaiah ,[1,2] Taek Su Lee,[1] Joong Hee Lee,[1] O. M. Samir,[3] R. Somashekar[3]

[1]*Bin Fusion Research Team, Department of Polymer and Nano Science and Technology, Chonbuk National University, Jeonju, Jeonbuk 561-756, South Korea*
[2]*Department of Polymer Science and Technology, Sri Jayachamarajendra College of Engineering, Mysore 570 006, India*
[3]*Department of Studies in Physics, University of Mysore, Mysore 570 006, India*

Received 12 September 2007; accepted 20 November 2007
DOI 10.1002/app.27847
Published online 21 March 2008 in Wiley InterScience (www.interscience.wiley.com).

ABSTRACT: Polyaniline/carboxylated multi-walled carbon nanotube (PAni/c-MWNT) nanocomposites have been synthesized by micellar aided emulsion polymerization with various c-MWNTs compositions, viz., 0.5, 1, 5, and 10 wt %. The microcrystalline parameters such as the nanocrystal size ($\langle N \rangle$), lattice strain (g), interplanar distance (d_{hkl}), width of the crystallite size distribution, surface weighted crystal size (D_s), and volume of the ordered regions were calculated from the X-ray data by using two mathematical models, namely the Exponential distribution and Reinhold distribution methods. The effects of heat ageing on the microcrystalline parameters of the PAni/c-MWNT nanocomposites were also studied and the results are correlated. The thermal stability and electrical resistivity of the PAni/c-MWNT nanocomposites were examined with thermogravimetric analysis (TGA) and a conventional two-probe method. The TGA data indicate that the thermal stability of the nanocomposites improved after the incorporation of c-MWNTs. The influence of temperature on the resistivity of the nanocomposites was also measured. © 2008 Wiley Periodicals, Inc. J Appl Polym Sci 109: 200–210, 2008

Key words: carbon nanotubes; polyaniline; nanocomposites; microcrystalline parameters; electrical resistivity; thermal stability

INTRODUCTION

Carbon nanotubes (CNTs) have attracted a great deal of interest in the scientific community because of their unique electronic, magnetic, mechanical, and gas adsorption properties.[1] Recently, several strategies have been proposed and developed to fabricate CNT-based devices with improved properties and functions.[2] Intense interest has been generated in harnessing the unique structure and outstanding properties of CNTs in various applications, for example hydrogen storage, super capacitors, biosensors, electromechanical actuators, and nanoprobes for high-resolution imaging and so on.[3,4] Among them, one of the most attractive propositions is to incorporate CNTs into polymer matrices to prepare high performance composites.[5] CNTs are quite effective fillers compared to traditional carbon black micro particles, primarily due to their high aspect ratios.[6] However, the main obstacle to the application of CNTs in composite materials is the difficulty of dispersing them in a polymeric matrix. As a result of their strong van der Waals interactions, the CNTs are tightly bundled in the form of ropes consisting of several tubes, thereby rendering them insoluble in aqueous and organic liquids, and thus unprocessable.[7] To unlock the potential of CNTs for use in polymer nanocomposites, much effort has been investigated over the last few years in an attempt to achieve a good dispersion method for CNTs in polymer matrices.

To improve the processability, electrical, magnetic, and optical properties of CNTs, conjugated or conducting polymers are attached to their surfaces by *in situ* polymerization. Among the various conducting polymers, polyaniline (PAni) is of particular interest in synthesizing polymer/CNT composites because of its environmental stability, good processability, and reversible control of the conductivity both by protonation and charge-transfer doping.[8,9] A considerable amount of progress has been made in designing and fabricating polyaniline/carboxylated multi-walled carbon nanotube (PAni/CNT) composites, because of their unique electrical properties as well as their extensive application in electronic devices.[10–12]

Correspondence to: J.-H. Lee (jhl@chonbuk.ac.kr).
Contract grant sponsors: Ministry of Education and Human Resources Development (Second Phase BK21 program); Chonbuk National University of Korea; Ministry of Commerce, Industry and Energy (MOCIE); Korea Industrial Technology Foundation (KOTEF).

Journal of Applied Polymer Science, Vol. 109, 200–210 (2008)

Recently, the synthesis and characterization of PAni/CNT nanocomposites has also been investigated.[13–17] Using this approach, PAni/CNT composite films have been fabricated by the chemical[18] or electrochemical[16] polymerization of aniline containing dissolved CNTs. Wan and coworkers synthesized PAni nanotubes doped with sulfonated CNTs via a self-assembly process.[19] Zhang et al. developed a cationic surfactant directed method to synthesize PAni/CNT nanocable composites.[10] Wu et al. obtained tubular PAni/CNT composites by *in situ* polymerization from carboxylic group capped CNTs.[20] Many researchers have characterized PAni/CNT nanocomposites using wide angle X-ray scattering and other analytical techniques.[13–20] For the commercial exploitation of nanocomposites, insight into their structure-property relationship is very important. However, a through literature survey reveals that there is a lack of information on the microcrystalline data of PAni/MWNT nanocomposites. The present study constitutes an attempt to interpret the X-ray patterns of nanocomposites using two different models, namely, the Exponential and Reinhold asymmetric column length distribution functions.

EXPERIMENTAL

Materials

MWNTs (diameter 10–20 nm, length 10–50 μm) produced by a catalytic vapor decomposition technique and with a purity of >95% were purchased from Iljin Nanotech Co., South Korea. Nitric acid (60% purity) was obtained from Aldrich Chemicals. Aniline (Ani) monomer (99% purity, Aldrich) was distilled under reduced pressure and stored at low temperature prior to use. Ammonium persulfate (APS), sodium dodecylsulfate (SDS), and all other organic solvents were of analytical grade and are used without further purification. The MWNTs were oxidized using concentrated nitric acid as per the procedure reported elsewhere.[21]

Preparation of PAni/c-MWNT nanocomposites

The PAni/c-MWNT nanocomposites were prepared by micellar aided emulsion polymerization. In a typical process, various amounts of c-MWNTs, viz., 0.5, 1, 5, and 10 wt % based on the aniline content were dispersed in chloroform using an ultrasonic bath for 30 min followed by the addition of 0.2*M* of SDS in aqueous media under vigorous stirring to form an emulsion. The precooled solution of aniline monomer (0.25*M*) was added to the above emulsion with constant stirring. To initiate the polymerization of aniline, APS (0.25*M*) solution was added dropwise over a period of 30 min with constant stirring. The aniline adsorbed on the surface of the c-MWNTs (core layer) was polymerized to form the outer shell of the CNTs. After 2 h the dark suspension turned green, indicating the formation of the emeraldine salt of PAni. The reaction was allowed to continue for 24 h at room temperature and the polymerization was terminated by pouring the reaction mixture into acetone, whereupon the PAni/c-MWNT composites precipitated out. The product formed was thoroughly washed with deionized water to remove the impurities such as unreacted monomer, excess SDS, and oxidant, and finally washed with acetone. Then, the product was dried in a vacuum oven at 60°C for 24 h.

Techniques

The electrical resistances of the PAni and PAni/c-MWNT nanocomposites were measured by the two-probe method at different temperatures. The temperature was monitored by using a controlled hot-air oven. The composite powder was compacted into a disk pellet with a diameter of 13.12 mm and thickness of 1.2 mm under a pressure of 20 MPa. A silver paste was coated on the surface of the specimens to obtain good contact with the electrodes. The resistance was measured at different temperatures by raising the temperature at a heating rate of 2°C/min from ambient to 200°C. Each data presented is the average value of the measurements from at least five samples.

Thermogravimetric analysis (TGA) of the PAni nanocomposites was carried out on a TA Instruments 2100 thermoanalytical system in the temperature range of 30–700°C with a heating rate of 10°C/min in air media. The X-ray diffraction (XRD) patterns were recorded on a Rigaku D/max 2500 Diffractometer at 40 kV, 30 mA, using Cu K_α monochromatic radiation with a wavelength of 1.5406 Å. The samples were scanned in the 2θ range of 5–50° at intervals of 0.03 employing a curved position sensitive detector in the transmission mode. These patterns were indexed using TREOR procedure. The intensity was corrected for Lorentz-polarization factors and also for instrumental broadening using Stokes deconvolution method. The microstructural parameters such as the crystal size ($\langle N \rangle$) and lattice strain (g in %) are determined by employing Fourier methods.[22–24] Different microcrystalline parameters were evaluated for PAni/MWNT composites from the X-ray profiles by two mathematical models, namely, the Exponential distribution and Reinhold distribution methods. The theory of the X-ray profile analysis to evaluate the crystalline parameters is reported in our previous communications.[25–27]

RESULTS AND DISCUSSION

X-ray diffraction

To probe the microstructure of these tubular nanocomposites, the powder X-ray diffraction (XRD) pat-

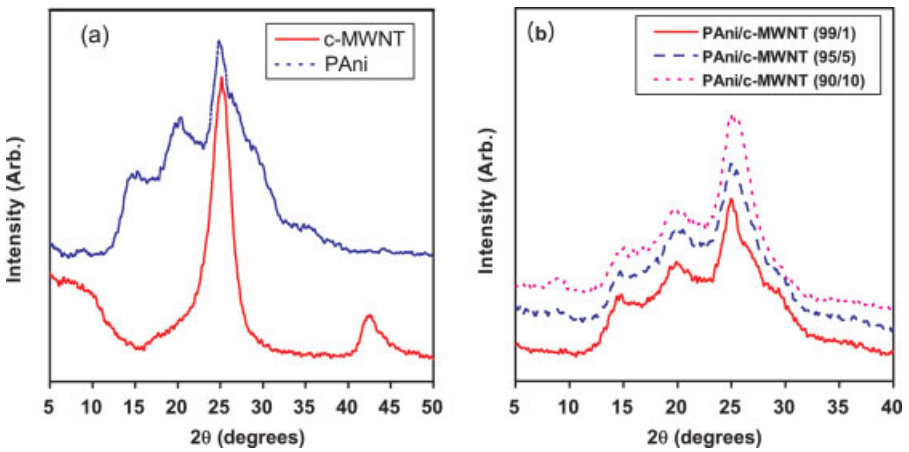

Figure 1 X-ray diffractograms of (a) PAni and c-MWNTs and (b) PAni/c-MWNT nanocomposites. [Color figure can be viewed in the online issue, which is available at www.interscience.wiley.com.]

TABLE I
Microstructural Parameters for PAni/c-MWNT Nanocomposites Determined Using Two Asymmetric Column Length Distribution Functions: (a) Exponential Distribution Function and (b) Reinhold Distribution Function

PAni/c-MWNTs (wt/wt %)	2θ (°)	d_{hkl} (Å)	$\langle N \rangle$	g (%)	D_s (Å)	δ	a/b*	Volume of the Ordered Regions (nm^3)
a. Exponential distribution function								
PAni	15.20	5.83	3.52	0.1	20.52	0.059	1.025	6.91
	20.40	4.35	7.51	0.1	32.67	0.152	0.945	
	24.82	3.59	2.87	0.1	10.30	0.101	1.239	
99.5/0.5	15.08	5.88	3.70	0.5	21.76	0.059	0.935	4.36
	20.48	4.34	4.53	1.0	19.66	0.126	0.565	
	25.28	3.52	2.89	0.1	10.17	0.084	0.879	
99/01	14.94	5.93	3.60	0.5	21.76	0.074	0.668	4.74
	20.28	4.38	5.04	0.1	22.08	0.196	0.917	
	25.02	3.56	2.77	0.1	9.86	0.083	0.860	
95/05	15.00	5.91	5.17	2.5	30.56	0.088	1.199	6.03
	20.04	4.43	4.36	0.1	19.31	0.147	0.561	
	25.00	3.56	2.87	0.1	10.22	0.094	0.762	
90/10	15.02	5.89	6.01	0.1	35.39	0.137	1.000	8.41
	20.00	4.43	5.04	0.5	22.33	0.095	0.424	
	25.00	3.56	2.99	0.1	10.64	0.058	0.601	
c-MWNTs	25.74	3.46	6.08	0.1	21.04	0.038	0.450	–
	43.00	2.10	8.60	0.5	18.06	0.052	0.202	
MWNTs	24.98	3.56	6.26	0.1	22.29	0.038	0.449	–
	42.28	2.14	8.24	0.1	17.63	0.083	0.407	
b. Reinhold distribution function								
PAni	15.20	5.83	3.51	0.1	20.46	0.060	1.366	6.89
	20.40	4.35	7.49	0.1	32.58	0.153	1.340	
	24.82	3.59	2.88	0.5	10.34	0.104	1.956	
99.5/0.5	15.08	5.88	3.70	0.5	21.76	0.060	1.339	4.14
	20.48	4.34	4.41	0.5	19.14	0.129	0.783	
	25.28	3.52	2.80	0.1	9.86	0.089	1.240	
99/01	14.94	5.93	3.54	0.1	20.99	0.071	0.941	4.51
	20.28	4.38	5.11	0.1	22.38	0.197	2.357	
	25.02	3.56	2.70	0.1	9.61	0.088	1.219	
95/05	15.00	5.91	5.04	0.5	29.79	0.089	1.549	4.91
	20.04	4.43	3.72	0.1	16.48	0.123	0.647	
	25.00	3.56	2.81	0.1	10.00	0.101	1.084	
90/10	15.02	5.89	6.01	0.5	35.39	0.139	.000	7.25
	20.00	4.43	4.86	1.0	21.53	0.095	0.576	
	25.00	3.56	2.67	0.1	9.51	0.065	0.794	
c-MWNTs	25.74	3.46	6.06	0.1	20.97	0.045	0.652	–
	43.00	2.10	8.02	0.5	16.84	0.056	0.278	
MWNTs	24.98	3.56	6.24	0.1	22.21	0.040	0.652	–
	42.28	2.14	8.19	0.1	17.53	0.086	0.606	

*a, for Exponential distribution function; b, for Reinhold distribution function.

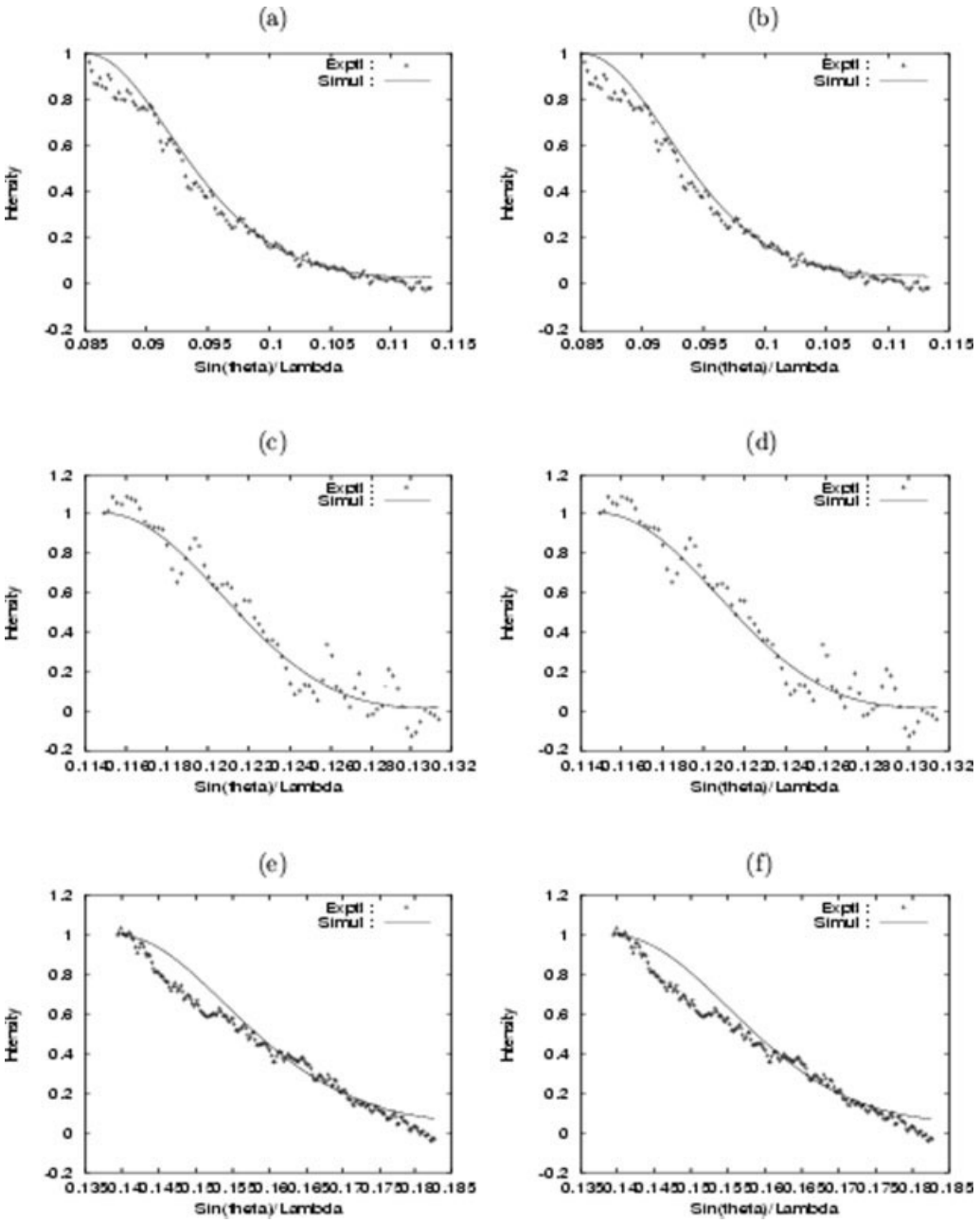

Figure 2 Experimental and simulated X-ray profiles for PAni using Exponential (a, c, e) and Reinhold distribution functions (b, d, f) at three different 2θ values.

terns of the MWNTs, c-MWNTs, PAni, and PAni/c-MWNT nanocomposites were recorded. The X-ray diffractograms of the PAni, c-MWNTs, and PAni/c-MWNT nanocomposites are shown in Figure 1. In the case of PAni, three peaks were observed at around $2\theta = 15^\circ$, 20°, and 25° [Fig. 1(a)]. The peak centered at $2\theta = 20^\circ$ may be ascribed to periodicity parallel to the polymer chain, while the peak at $2\theta = 25^\circ$ may be due to the periodicity perpendicular to the polymer chain.[28] The peak at $2\theta = 20^\circ$ also represents the characteristic distance between the ring planes of benzene rings in adjacent chains or the close contact interchain distance.[29] For PAni-SDS complex, the peak at $2\theta = 25^\circ$ is stronger than that of $2\theta = 20^\circ$, which is similar to that of doped emeraldine salt.[30] The intense peak that appeared at around $2\theta = 25^\circ$ is a relatively sharp, well-defined peak, and the other two peaks are also due to the Bragg-like order of the material associated with paracrystalline disorder.[31]

The microcrystalline parameters such as the interplanar spacing (d_{hkl}), nanocrystal size ($\langle N \rangle$), lattice

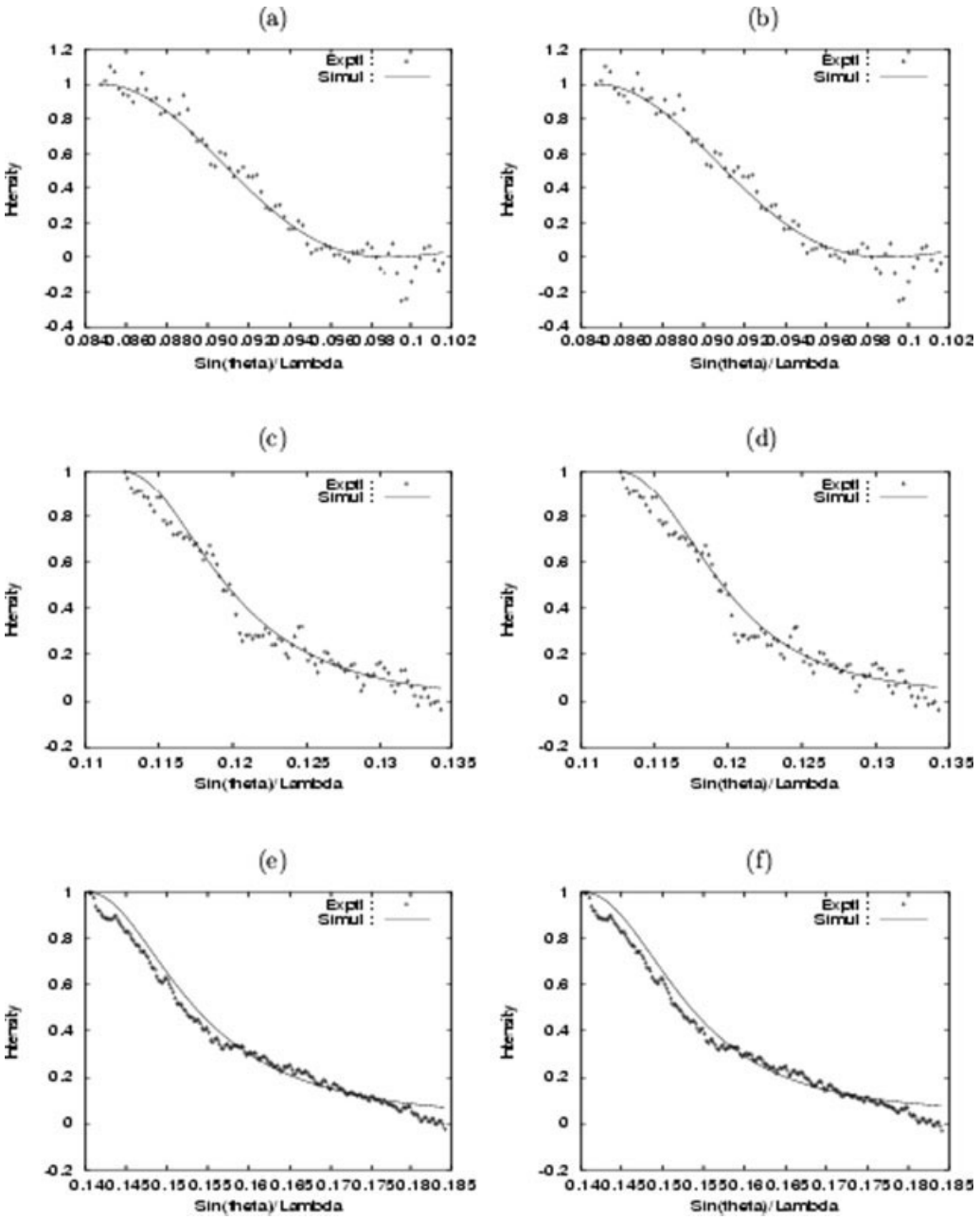

Figure 3 Experimental and simulated X-ray profiles for PAni/c-MWNTs (90/10) using Exponential (a, c, e) and Reinhold distribution functions (b, d, f) at three different 2θ values.

strain (g in %), surface weighted crystal size (D_s), and volume of the ordered regions for the PAni, c-MWNTs and PAni/c-MWNT nanocomposites were calculated using Exponential and Reinhold asymmetric distribution functions and the results are given in Table I. The Bragg peak at 24.82° with lattice spacing (d) of 3.59 Å suggests that the dodecyl group of SDS can act as a counter ion in the doping of the PAni. In the case of the c-MWNTs, peaks were observed at 2θ = 24.98° and 42.28° with spacing of 3.56 Å and 2.14 Å, corresponding to a graphite-like diffraction and small amounts of catalytic particles encapsulated inside the walls of the c-MWNTs, respectively, [Fig. 1(a)].[32] The c-MWNTs showed lower values of $\langle N \rangle$ and D_s as compared to the MWNTs. This is due to the reduction in the order structure of the MWNTs after the incorporation of the bulky carboxylic groups into the walls of the nanotubes. The formation of the tubular composite is indicated by the enhancement of the intensity of the peaks at 2θ = 15°, 20°, and 25° [Fig. 1(b)] and, hence, from the structural point of view, no additional order has been introduced. The increase in the intensity of the peak at 25° with increasing c-MWNTs concentration is due to the increase in the doping level. Because of the small mass fraction at a lower concentration, the

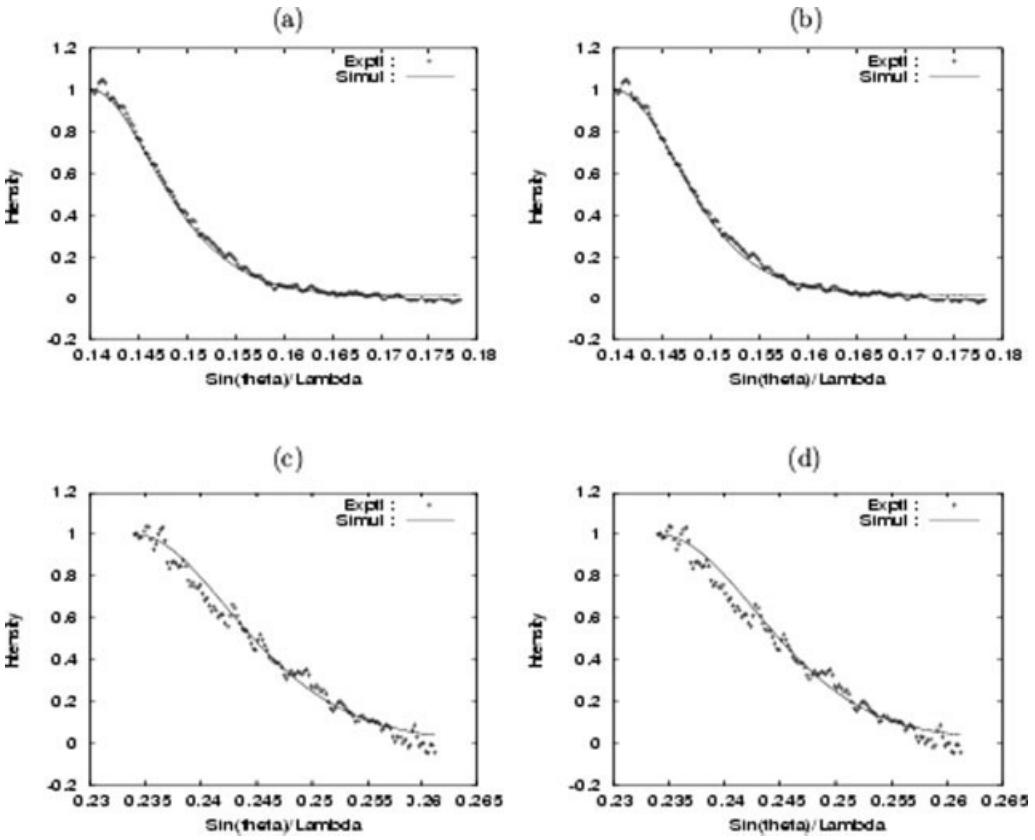

Figure 4 Experimental and simulated X-ray profiles for c-MWNTs using Exponential (a, c) and Reinhold distribution functions (b, d) at two different 2θ values.

graphite-like diffraction peaks of the c-MWNTs in the tubular composite can hardly be detected. Therefore, the relative increase in the intensity of the crystalline peaks comes from the presence of c-MWNTs in the tubular composite. In other words, although there is a very thin amorphous layer on the surface of the c-MWNTs, the c-MWNTs easily order the PAni macromolecule along their axis and, thus, the percentage crystallinity of the outer layer of the tubular composite increases. Since there are three different Bragg reflections, we can define the order along these directions and, hence, the volume of composites which specifies crystalline order. This volume is given by the product of the crystallite sizes measured by line profile analysis for these three Bragg reflections. From Table I, it was noticed that the volume of the ordered regions increases with increasing c-MWNTs content. The volume of the ordered regions represents those regions in the polymer network which contribute to the X-ray Bragg reflections. In real space, essentially, a lower number of columns participate in the Bragg-like diffraction process. In reciprocal space, much broadening of the reflection at $2\theta = 25^\circ$ is observed. The increase in the intensity of the X-ray ($2\theta = 25^\circ$) with increasing c-MWNT content can be attributed to the concentration of MWNTs, which have higher scattering factors. The fact that the lattice spacing corresponds to ~3.50 Å ($2\theta = 25^\circ$) indicates that there is an increase in inter- and intra-molecular weak hydrogen bond formed between the PAni and c-MWNTs. The measured full width and half maxima of the reflection at $2\theta = 24.82^\circ$ is 2.82 for PAni and 2.95, 2.71, 4.06, and 4.64 for the 0.5, 1, 5, and 10% c-MWNT composites, respectively. The increase in the width of the reflection in reciprocal space is equivalent to a decrease in the crystalline order in direct space. This increase in intensity is due to the increase in the concentration of c-MWNTs in the matrix with their higher scattering factor.

To ascertain the most suitable asymmetric distribution, a fitness test was conducted using line profile simulation from the peak of the reflection to its baseline. The experimental and simulated X-ray profiles for the PAni and PAni/c-MWNT nanocomposites calculated using all the distribution functions and specimen profiles for the PAni, PAni/c-MWNT (90/10) nanocomposites (three peaks), and for c-MWNTs (two peaks) are shown in Figures 2–4 respectively. It is evident from these figures that there is good agreement between the experimental and theoretically calculated X-ray data for the Expo-

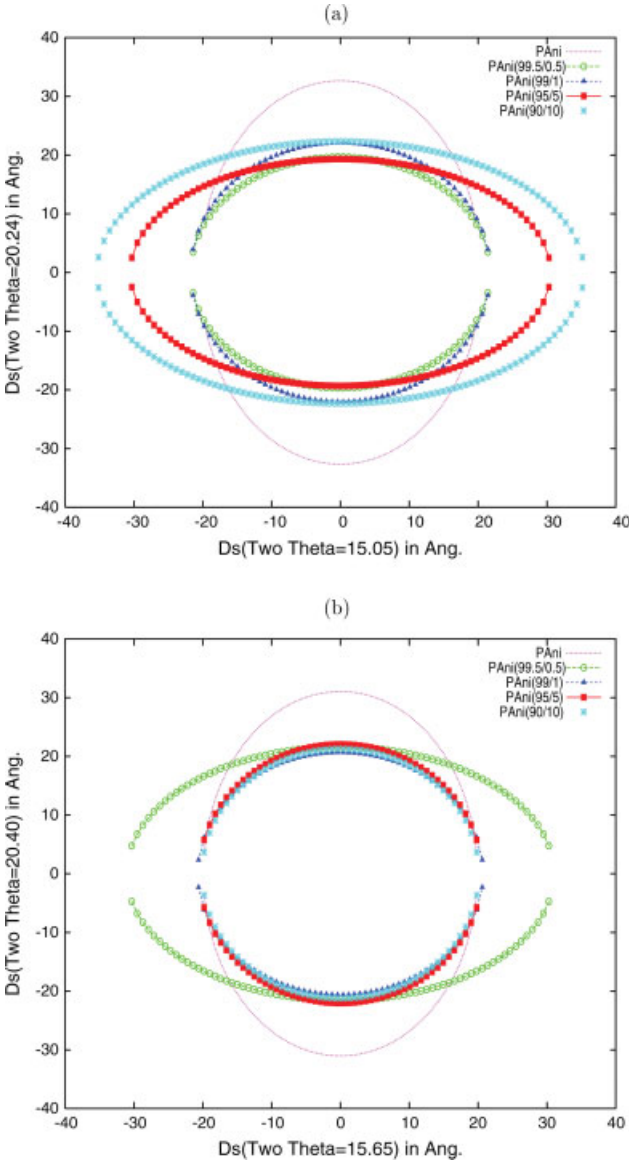

Figure 5 The crystallite size ellipse for the PAni and PAni/c-MWNT nanocomposites, (a) before and (b) after thermal treatment. [Color figure can be viewed in the online issue, which is available at www.interscience.wiley.com.]

nential distribution function. In all cases, the goodness of fit was less than 15%. These results are further justified by the behavior of the microstructural quantities such as the crystal size or correlation length ($\langle N \rangle$) and lattice strain (g) at the microscopic level (Table I). There was no systematic variation of the $\langle N \rangle$, g, and D_s values with the compositions of PAni/c-MWNT nanocomposites. The D_s results clearly indicated that the degree of crystallinity present at the surface was almost the same for all of the formulations. The physical interpretation of the crystal imperfection parameters such as $\langle N \rangle$ and g essentially indicated the deviation in the lattice ordering for a distance of $D = Nd_{hkl}$ (Å) along the direction normal to the Bragg (hkl) plane. The variation in the D_s values of the nanocomposites is due to the change in the morphology of the c-MWNTs after their coating with PAni. However, the interplanar distance of the main peak was found to be lower than the corresponding value of the less intense peaks, whereas the variation is the same. This implies that there is a change in the structure of the composite system after coating.

From Table I, it is also evident that the Exponential distribution has a smaller standard deviation (δ) than the other distribution function and, hence, we have preferred the corresponding results for further interpretation. The terms α and β are the width of the Exponential distribution and the width of the Reinhold distribution, respectively. These distributions are those of the crystallite size in the phase. The intensity of the scattered X-rays depends on the settings. It is the shape of the profile that is evaluated by the different models. If these are small, it implies a sharp distribution function in which the system has a unique set of crystallites. If these are large, it implies a wide distribution function, which essentially implies that the system has crystallites of various sizes and shapes. It is evident from Table I that the width of the crystallite distribution decreases with the increase in the c-MWNTs.

The computed microstructural parameters were used for computing the shape of the coherent domains in the form of ellipsoids using the surface weighted crystal size (D_s) values, corresponding to the average 2θ values along the x and y axes, respectively, and the same is shown in Figure 5(a). From this figure, it is evident that there are significant changes only in the periphery of the crystallite shape ellipsoid for the PAni/c-MWNT nanocomposites.

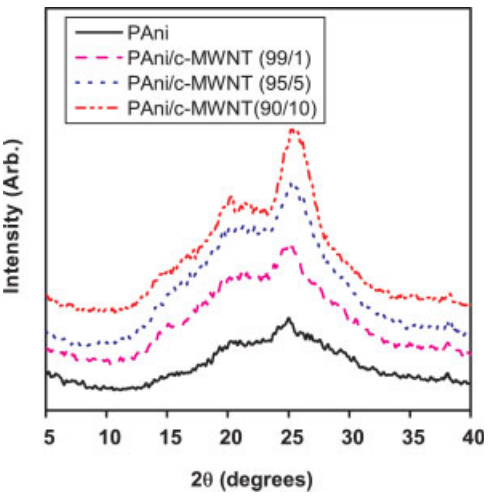

Figure 6 X-ray profiles of thermally treated PAni and PAni/c-MWNT nanocomposites. [Color figure can be viewed in the online issue, which is available at www.interscience.wiley.com.]

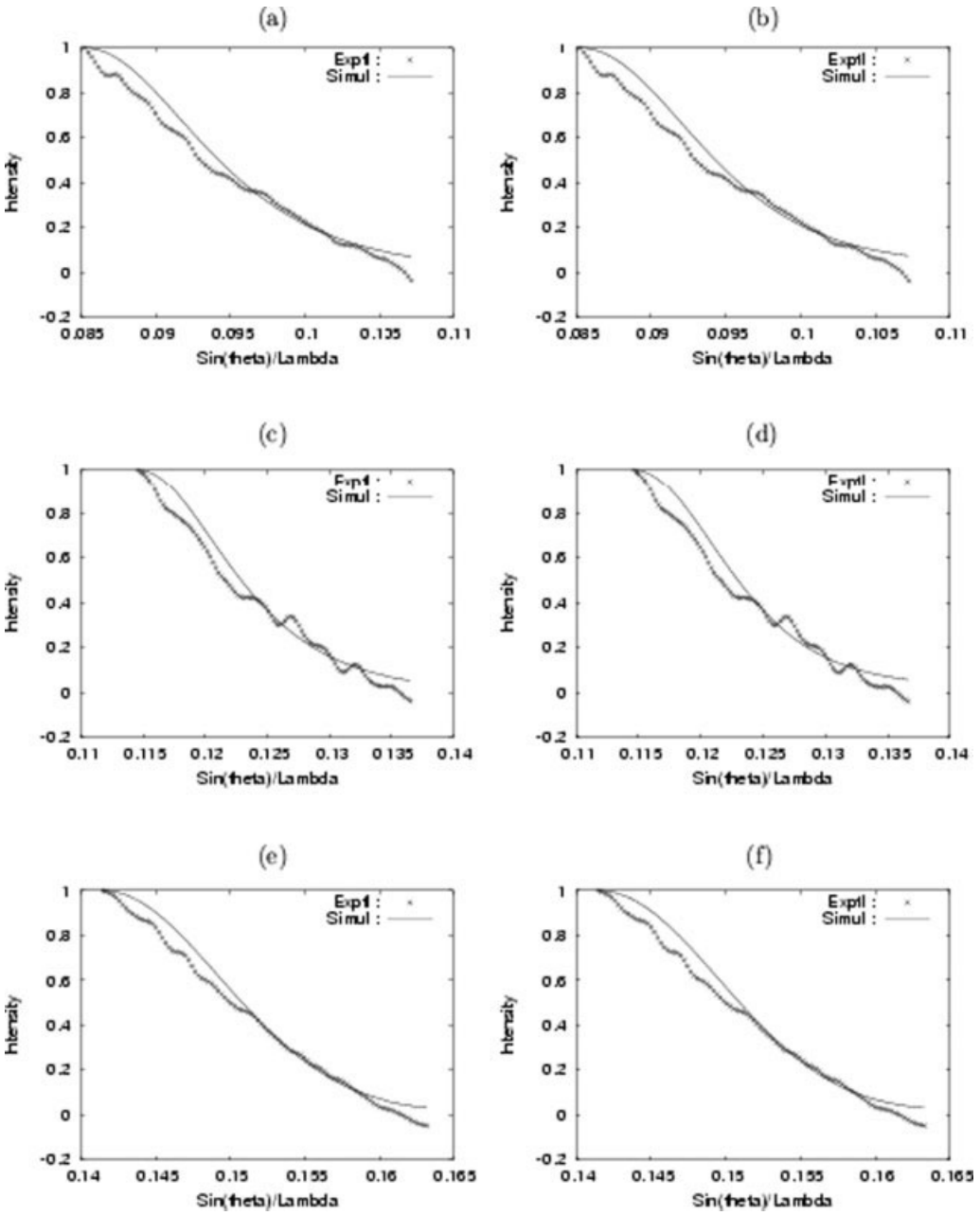

Figure 7 Experimental and simulated X-ray profiles for thermally treated PAni/c-MWNTs (90/10) using Exponential (a, c, e) and Reinhold distribution functions (b, d, f) at three different 2θ values.

From this figure, it was also noticed that the crystallite size ellipse increases with increasing c-MWNT content in the composites, as expected. According to Hosemann's model, these changes in the crystal size values as well as the shape ellipsoids are attributed to the interplay between the strain present in the polymer network and the number of unit cells coherently contributing to the X-ray reflection.

The PAni/c-MWNT nanocomposites were exposed to a temperature of 200°C for 4 h and the effect of the heat treatment on their crystalline behavior was measured using XRD (Fig. 6). The experimental and simulated X-ray profiles for the thermally treated nanocomposites calculated using both the distribution functions and specimen profiles for the PAni/c-MWNTs (90/10) for all peaks are shown in Figure 7. It is evident from this figure that there is a good agreement between the experimental and theoretically calculated X-ray data for the Exponential distribution functions. In all cases, the goodness of the fit was less than 15%. The microcrystalline parameters calculated using the Exponential and Reinhold distribution functions for the heat-aged nanocomposites are given in Table II. The nanocrystal size ($\langle N \rangle$) and volume of the ordered regions values are larger for the thermally treated samples than the untreated composites. However, there is no systematic

TABLE II
Microstructural Parameters for Thermally Treated PAni/c-MWNT Nanocomposites Determined Using Two Asymmetric Column Length Distribution Functions: (a) Exponential Distribution Function and (b) Reinhold Distribution Function

PAni/c-MWNTs (wt/wt %)	2θ (°)	d_{hkl} (Å)	$\langle N \rangle$	g %	D_s (Å)	δ	a/b*	Volume of the Ordered Regions (nm^3)
a. Exponential distribution function								
PAni	16.29	5.43	3.67	0.1	19.94	0.094	1.000	20.20
	20.78	4.27	7.24	0.1	31.04	0.092	1.000	
	24.98	3.56	9.16	0.5	32.63	0.118	0.208	
99.5/0.5	14.94	5.93	5.24	0.5	31.07	0.065	0.505	21.65
	20.02	4.43	4.87	0.5	21.57	0.088	0.603	
	24.92	3.57	9.05	0.1	32.31	0.109	0.286	
99/01	15.46	5.73	3.62	0.1	20.74	0.082	0.807	9.28
	20.16	4.40	5.56	0.1	20.06	0.071	0.805	
	24.89	3.57	6.25	0.1	22.31	0.079	0.449	
95/05	16.50	5.37	5.82	0.1	20.51	0.067	1.000	9.69
	20.72	4.28	5.15	0.5	22.04	0.056	1.000	
	25.26	3.52	6.09	0.5	21.44	0.067	0.556	
90/10	15.10	5.86	3.43	0.5	20.10	0.061	0.829	9.32
	20.34	4.36	4.87	0.5	21.23	0.079	0.561	
	25.18	3.53	6.19	0.5	21.85	0.062	0.749	
b. Reinhold distribution function								
PAni	16.29	5.43	3.67	0.1	19.93	0.094	1.000	18.28
	20.78	4.27	7.26	0.1	31.00	0.092	1.000	
	24.98	3.56	8.31	0.1	29.58	0.124	0.278	
99.5/0.5	14.94	5.93	5.20	0.5	30.84	0.072	0.735	20.94
	20.02	4.43	4.84	0.5	21.44	0.093	0.880	
	24.92	3.57	8.87	0.1	31.67	0.113	0.400	
99/01	15.46	5.73	3.58	0.5	20.51	0.084	1.156	9.03
	20.16	4.40	4.54	0.1	19.98	0.074	1.183	
	24.89	3.57	6.17	0.1	22.03	0.085	0.639	
95/05	16.50	5.37	3.82	0.1	20.51	0.067	1.000	9.66
	20.72	4.28	5.15	0.1	22.04	0.059	1.000	
	25.26	3.52	6.07	0.5	21.37	0.071	0.814	
90/10	15.10	5.86	3.41	1.0	19.98	0.067	1.181	9.14
	20.34	4.36	4.81	0.5	20.97	0.085	0.797	
	25.18	3.53	6.18	0.1	21.82	0.064	1.162	

*a, for Exponential distribution function; b, for Reinhold distribution function.

variation in the volume of the ordered regions of the nanocomposites after the thermal treatment. A marked increase in the D_s values is also noticed for the reflection at $2\theta = 25^\circ$ after the thermal treatment. These results clearly indicate that there is an increase in the crystallinity of the nanocomposites after they have been subjected to the heat treatment. This is because, after the heat treatment, the nanocomposites are free from volatile impurities such as water, excess dopant, unreacted monomer, solvent, etc. This change in the composition influences the molecular reordering of the PAni-coated MWNT system, which causes an increase in $\langle N \rangle$ and D_s. The crystallite size ellipses for the heat-aged PAni and PAni/c-MWNT nanocomposites are shown in Figure 5(b). From this figure, it was evident that there are significant changes only in the periphery of the crystallite shape ellipsoid.

Thermal behavior

The thermal stability of the PAni, c-MWNTs, and PAni/c-MWNT composites were examined by TGA. The TGA thermograms for the PAni, PAni/c-MWNTs, and c-MWNTs are shown in Figure 8. The TGA thermogram of the c-MWNTs showed a slight reduction in weight in the temperature range of 100–500°C. This may be due to the presence of moisture and other impurities in the functionalized MWNTs. The TGA and its derivative thermograms for the PAni, PAni/c-MWNTs (90/10), and c-MWNTs are shown in Figure 9(a–c) respectively. The c-MWNTs undergo one step thermal degradation, which occurs in the temperature range of 517–695°C with a major weight loss of 98%. On the other hand, the PAni and PAni/c-MWNT nanocomposites undergo four-step thermal degradation processes. In the first step of degradation, a small fraction of weight loss occurs in the temperature range of 70–190°C, which is due to the expulsion of the moisture present in the PAni.[33] The second step weight loss occurs in the temperature range of 220–340°C, which is due to the loss of unbounded dopant (SDS) and oligomers. Then, a very significant

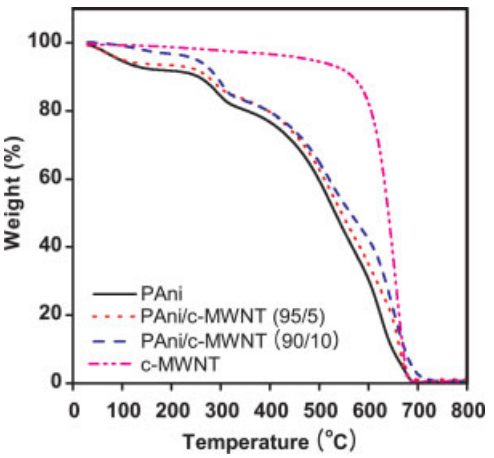

Figure 8 TGA thermograms for PAni, PAni/c-MWNT nanocomposites, and c-MWNTs. [Color figure can be viewed in the online issue, which is available at www.interscience.wiley.com.]

weight loss occurs in the third and fourth steps in the temperature ranges of 369–566°C and 580–744°C, which is due to the loss of the bounded dopant and thermal oxidative decomposition of the nanocomposites respectively.[34] From these figures, the high thermal stability of the c-MWNTs and low thermal stability of PAni can be seen. This is because the CNTs constitute an inorganic component and PAni is a hydrophilic organic compound. The increased thermal stability of PAni/MWNT composites over that of the pure PAni is likely to be a result of absorption, by the activated CNT surface, of free radicals generated during polymer decomposition.[34]

Electrical properties

The plot of the electrical resistivity against temperature for the PAni and PAni-coated c-MWNTs are shown in Figure 10. Obviously, the pure PAni has a high resistivity at room temperature as compared to its nanocomposites. The room temperature electrical resistivity of the nanocomposites decreases with increasing c-MWNT content, due to dopant effect caused by c-MWNTs. MWNTs are relatively good electron acceptors, while PAni can be considered as a good electron donor. From Figure 10, it was also noticed that, up to 125°C, the resistivity of PAni and its nanocomposites are not affected by temperature. However, a steep increase in the re-

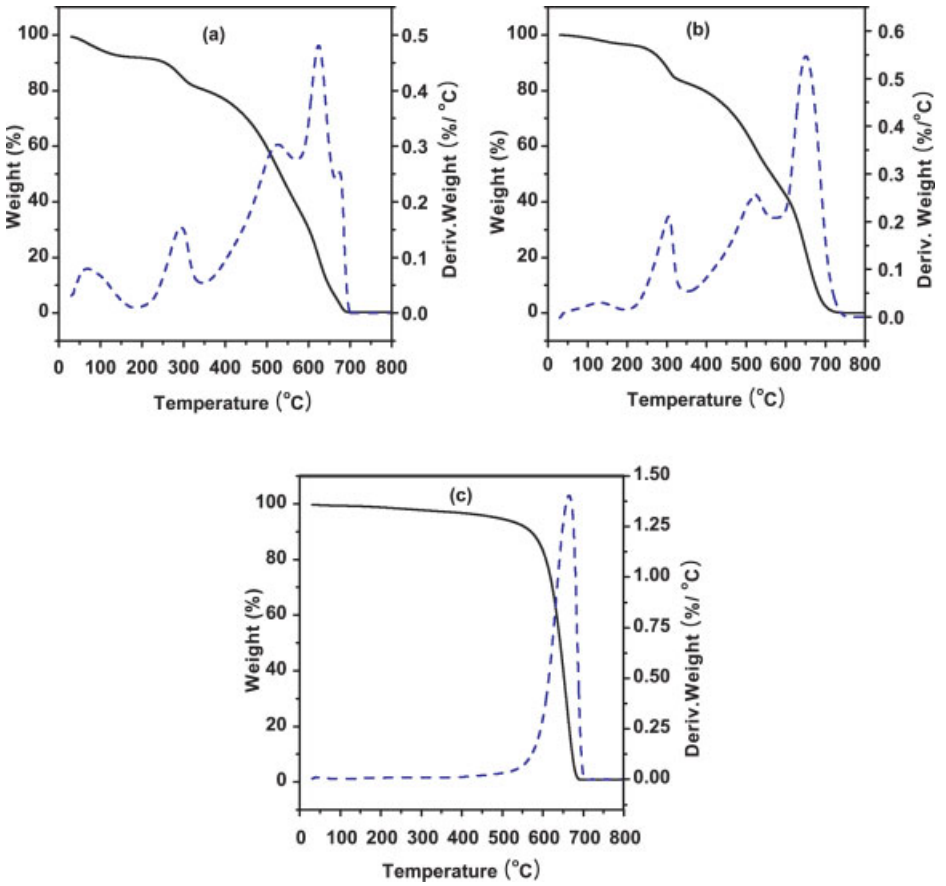

Figure 9 TGA and its derivative thermograms of, (a) PAni, (b) PAni/c-MWNTs (90/10), and (c) c-MWNTs. [Color figure can be viewed in the online issue, which is available at www.interscience.wiley.com.]

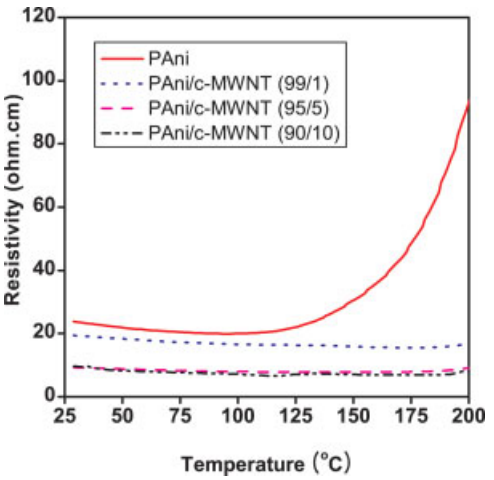

Figure 10 Plot of resistivity against temperature for PAni and PAni/c-MWNT nanocomposites. [Color figure can be viewed in the online issue, which is available at www.interscience.wiley.com.]

sistivity of PAni was noticed above 125°C, which may be due to the loss of moisture and the degradation of excess SDS. On the other hand, the PAni coated c-MWNTs retains the same resistivity throughout the measured temperature range. This behavior is due to the charge transfer interaction between the external PAni shell layer and the internal c-MWNTs.[35,36] This result clearly indicates that the PAni/c-MWNT nanocomposites can be used up to 200°C.

CONCLUSIONS

The structure-property relationships of PAni/c-MWNT nanocomposites were estimated using X-ray profile. The X-ray results revealed that there is an increase in the crystallite size ellipse and volume of the ordered regions (4.14–8.41 nm^3) with increasing c-MWNT content in the nanocomposites. The effects of heat ageing on the microcrystalline parameters of the nanocomposites were measured. A marked increase in the nanocrystal size ($\langle N \rangle$), volume of the ordered regions, and D_s (at $2\theta = 25^\circ$) values for the thermally treated samples as compared to the corresponding untreated nanocomposites was noticed. These results confirm the reordering in the polymer network after heat treatment. The influence of temperature on the electrical resistivity of the PAni/c-MWNT nanocomposites is insignificant. From the TGA data, it can be concluded that the nanocomposites are thermally stable. All these parameters indicate that, the fabricated PAni-coated MWNT nanocomposites might constitute useful materials for various applications, e.g., in fuel cells, thermistors, self regulating heaters, supercapacitors, sensors, in batteries as cathode, etc.

References

1. Iijima, S. Nature 1991, 354, 56.
2. Charlier, J. C.; Terrones, M.; Baxendale, M.; Meunier, V.; Zacharia, T.; Rupesinghe, N. L.; Hsu, W. K.; Grobert, N.; Terrones, H.; Amaratunga, G. A. J. Nano Lett 2002, 2, 1191.
3. Baughman, R. H.; Zakhidov, A. A.; Heer, W. A. D. Science 2002, 297, 787.
4. Esplandiu, M. J.; Bittner, V. G.; Giapis, K. P.; Collier, C. P. Nano Lett 2004, 4, 1873.
5. Barraza, H. J.; Pompeo, F.; O'Rear, E. A.; Resasco, D. E. Nano Lett 2002, 2, 797.
6. Andrews, R.; Weisenberger, M. C. Solid State Mater Sci 2003.
7. Thostenson, E. T.; Ren, Z.; Chou, T. W. Compos Sci Technol 2001, 61, 1899.
8. MacDiarmid, A. G.; Chiang, J. C.; Richter, A. F. Synth Met 1987, 18, 285.
9. Cao, Y.; Smith, P.; Heeger, A. J. Synth Met 1992, 48, 91.
10. Zhang, X. T.; Zhang, J.; Wang, R. M.; Liu, Z. F. Carbon 2004, 42, 1455.
11. Long, Y. Z.; Chen, J. Z.; Zhang, X. T.; Zhang, J.; Liu, Z. F. Appl Phys Lett 2004, 85, 1796.
12. Ramamurthy, P. C.; Malshe, A. M.; Harrell, W. R.; Gregory, R. V.; Mcguire, K.; Rao, A. M. Solid State Electron 2019 2004, 48.
13. Zengin, H.; Zhou, W.; Jin, J.; Czerw, R.; Smith, J.; Dennis, W.; Echegoyen, L.; Carroll, D. L.; Foulger, S. H.; Ballato, J. Adv Mater 2002, 14, 1480.
14. Baibarac, M.; Baltog, I.; Lefrant, S.; Mevellec, J. Y.; Chauvet, O. Mol Cryst Liq Cryst 2004, 415, 141.
15. Deng, J.; Ding, X.; Zhang, W.; Peng, Y.; Wang, J.; Long, X.; Li, P.; Chan, A. S. C. Eur Polym Mater 2002, 38, 2497.
16. Huang, J. E.; Li, X. H.; Xu, J. C.; Li, H. L. Carbon 2003, 41, 2731.
17. Sainz, R.; Benito, A. M.; Martnez, M. T.; Galindo, J. F.; Sotres, J.; Bar'o, A. M.; Corraze, B.; Chauvet, O.; Maser, W. K. Adv Mater 2005, 17, 278.
18. Li, X. H.; Wu, B.; Huang, J. E.; Zhang, J.; Liu, Z. F.; Li, H. Carbon 2002, 41, 1670.
19. Wei, Z. X.; Wan, M. X.; Lin, T.; Dai, L. M. Adv Mater 2003, 15, 136.
20. Wu, T. M.; Lin, Y. W.; Liao, C. S. Carbon 2005, 43, 734.
21. Jeevananda, T.; Siddaramaiah; Kim, N.-H.; Heo, S.-B.; Lee, J.-H. Polym Adv Technol, submitted.
22. Warren, B. E.; Averbach, B. L. J Appl Phys 1950, 21, 595.
23. Warren, B. E. Acta Cryst 1955, 8, 483.
24. Warren, B. E. X-ray Diffraction; Addison-Wesley: New York, 1969.
25. Kumar, H.; Siddaramaiah; Somashekar, R.; Mahesh, S. S. Mater Sci Eng A 2007, 447, 58.
26. Kumar, H.; Siddaramaiah; Somashekar, R.; Mahesh, S. S. Eur Polym Mater 2007, 43, 611.
27. Somashekar, R.; Somashekarappa, H. J Appl Cryst 1997, 30, 147.
28. Moon, Y. B.; Cao, Y.; Smith, P.; Heeger, A. J Polym Commun 1989, 30, 196.
29. Pouget, J. P.; Hsu, C. H.; MacDiarmid, A. G.; Epstein, A. J. Synth Met 1995, 69, 119.
30. Pouget, J. P.; Jozefowicz, M. E.; Epstein, A. J.; Tang, X.; MacDiarmid, A. G. Macromolecules 1991, 24, 779.
31. Chaudhari, H. K.; Kelkar, D. S. Polym Int 1997, 42, 380.
32. Liu, S. W.; Yue, J.; Wehmschulte, R. J. Nano Lett 2002, 2, 1439.
33. Jeevananda, T.; Siddaramaiah; Seetharamu, S.; Saravanan, S.; D'Souza, L. Synth Met 2004, 140, 247.
34. Shaffer, S. P.; Windle, A. H. Adv Mater 1999, 11, 937.
35. Feng, W.; Bai, X. D.; Lian, Y. Q.; Liang, J.; Wang, X. G.; Yoshino, K. Carbon 2003, 41, 1551.
36. Cao, J.; Sun, J. Z.; Hong, H.; Li, H. Y.; Chen, H. Z.; Wang, M. Adv Mater 2004, 16, 84.